IEEE Access
Multidisciplinary | Rapid Review | Open Access Journal

Received September 9, 2016, accepted September 22, 2016, date of publication September 27, 2016, date of current version November 8, 2016.

Digital Object Identifier 10.1109/ACCESS.2016.2613883

Wideband Filtering Power Divider With Ultra-Wideband Harmonic Suppression and Isolation

YONGLE WU[1], (Senior Member, IEEE), ZHENG ZHUANG[1], YUANAN LIU[1], LI DENG[2], AND ZABIH GHASSEMLOOY[3], (Senior Member, IEEE)

[1]Beijing Key Laboratory of Work Safety Intelligent Monitoring, School of Electronic Engineering, Beijing University of Posts and Telecommunications, Beijing 100876, China
[2]Beijing Key Laboratory of Network System Architecture and Convergence, School of Information and Communication Engineering, Beijing University of Posts and Telecommunications, Beijing 100876, China
[3]NCR Laboratory, Optical Communications Research Group, Faculty of Engineering and Environment, Northumbria University, Newcastle upon Tyne, NE1 8ST, U.K.

Corresponding author: Y. Wu (wuyongle138@gmail.com)

This work was supported in part by the National Key Basic Research Program of China (973 Program) under Grant 2014CB339900 and in part by the National Natural Science Foundation of China under Grant 61422103 and Grant 61671084.

ABSTRACT In this paper, a wideband filtering power divider (PD) with ultra-wideband harmonic suppression and isolation is proposed. The dual coupled-line sections are embedded to the conventional quarter-wavelength transmission lines, which helps to extend the passband of the PD. With the introduction of the short-circuit stubs shunted at the output ports and the coupled lines with the open-circuit stubs, the ultra-wide stopband can be implemented more efficiently, thus resulting in five transmission zeros from 2 to 6 GHz. Furthermore, the improved isolation structure with series connected a resistor and a capacitor can be utilized to realize the ultra-wide isolation frequency band. Using a single resistor between two output ports, we have achieved an excellent in-band isolation. For demonstration, a wideband filtering PD operating at 1 GHz with a 20-dB bandwidth of 50% and an ultra-wide stopband better than 20 dB from 2 to 6 GHz is designed, fabricated, and measured. The measured results agree well with the anticipation.

INDEX TERMS Filtering power divider, harmonic suppression, ultra-wideband, coupled-line, improved isolation.

I. INTRODUCTION

In modern wireless communication systems, the ever increasing demand for the low cost and miniaturized high-performance radio frequency (RF)/microwave components has led to growing volume of investigations for multifunctional microwave devices. Owing to the indispensability of the power dividers (PDs) and filters in RF/microwave front end devices, much attention has been extensively paid to the PDs with high passband frequency selectivity [1]–[10].

The PD with two bandpass filters embedded in quarter-wavelength transmission lines (TLs) sections has been employed to achieve the desired filtering response and improve frequency selectivity [1]. However, the designed circuit has poor insertion loss and isolation between the output ports. In order to improve the isolation property, a parallel inductor-capacitor (*LC*) resonator is loaded onto the isolation network for minimizing the divergence between even- and odd-mode impedances around the passband at the cost of a narrow operating frequency band [2]. In addition, the compact folded quarter-wavelength resonators are applied in highly symmetric coupling structures for improved in-band isolation, which is difficult for accurate fabrication [3]. Although the aforementioned improvements to date are substantial and inspiring, the out-of-band interference up to harmonic frequencies has not been considered, which limits the application of such devices in a multi-standard wireless communication system.

In order to create the wide stopband suppressing the out-of-band interference, two dual-mode resonators [4] and four discriminating coupled resonators [5] are loaded in quarter-wavelength TLs for generating the desired filtering response and the out-of-band transmission zeros. Additionally, by employing the short-circuited half-wavelength resonators [6] and spiral resonators [7], the harmonic suppression

functionality can be combined in PDs. Nevertheless, the main disadvantages of these PDs with a wide stopband are the narrow passband [4], [5] and poor isolation [6], [7]. For developing wideband filtering PDs with a wide stopband and an isolation frequency band, the quasi-coupled lines with a complex matching isolation network and open-/short-circuit stubs are utilized [8]. Although the bandwidth of the isolation and stopband are acceptable, the in-band return loss and the level of harmonic suppression need further improvement. Besides the single-band equal filtering power division ratio case, other responses have also been investigated, including unequal power division [9], the dual passband operation [10], tunable filtering [11] and multi-way property [12], [13].

In this paper, a novel wideband filtering PD is proposed with many advanced properties including excellent in-band return loss, high in-band isolation, good harmonic suppression, ultra-wide isolation frequency band, and ultra-wide stopband, which is composed of two coupled-line (CL) sections, short-circuit stubs, and coupled lines with open-circuit stubs. The two-section CLs based on the centre-loaded coupled structures with open-circuit stubs are used to extend the passband while the short-circuit stubs can achieve the ultra-wide stopband with five transmission zeros. In addition, the ultra-wide isolation frequency band and high in-band isolation can be realized by the improved isolation structure with a series connected resistor and capacitor and a single resistor between two output ports. Finally, the complete design theories, procedures and results for the proposed PDs are also provided in details.

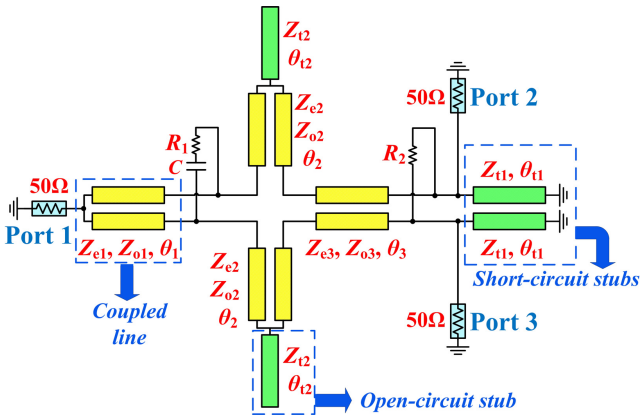

FIGURE 1. The schematic diagram of the proposed wideband filtering power divider.

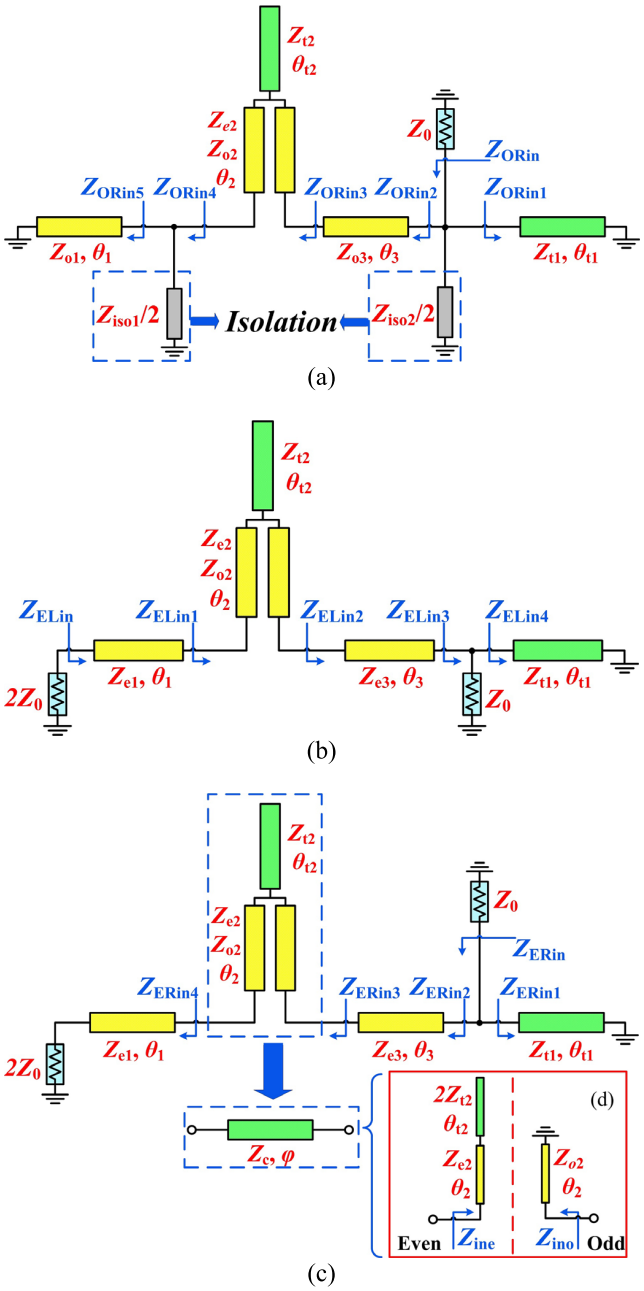

FIGURE 2. Equivalent circuits of the proposed filtering power divider in Fig. 1: (a) odd mode with right-hand side excitation; (b) Even mode with left-hand side excitation. (c) even mode with right-hand side excitation; (d) the odd-/even-mode circuit of the coupled lines with open-circuit stub, which is equivalent to a TL with a characteristic impedance Z_c and an electrical length φ.

II. DESIGN METHODOLOGY

A. ODD-/EVEN-MODE ANALYSIS

Fig. 1 depicts the designed wideband filtering power divider (WFPD) circuit configuration, which is composed of two CL sections, the short-circuit stubs, and the CLs with open-circuit stubs. As shown in Fig. 2, the S-parameters of the proposed WFPD can be obtained based on the odd-/even-mode analysis. For simplicity, CLs with open-circuit stubs are equivalent to a TL in Fig. 2(c). Moreover, the odd-/even-mode circuits of CLs with open-circuit stubs are illustrated in Fig. 2(d). Since microstrip lines at high frequency exist in the quasi-TEM mode, the phase velocities of the even and odd modes are not equal in general. However, because the coupling of the coupled-line structures in this work is not very strong, all the coupled-line structures can be reasonably assumed to have the same even-/odd-mode electrical lengths.

First, the electrical lengths of all the TLs shown in Fig. 2 satisfy the following condition: $\theta_1 = \theta_2 = \theta_3 = \theta_{t2} = \theta = \pi/8$, except for the short-circuit stub with the electrical length of $\pi/2$ (i.e. $\theta_{t1} = 4\theta$). Therefore, the odd-/even-mode input impedances of the CLs with open-circuit stubs can be expressed as

$$Z_{ine} = jZ_{e2}\frac{Z_{e2}\tan\theta - 2Z_{t2}\cot\theta}{Z_{e2} + 2Z_{t2}}, \tag{1a}$$

$$Z_{ino} = jZ_{o2}\tan\theta, \tag{1b}$$

where Z_{e2} and Z_{o2} are the even- and odd-mode characteristic impedances of the coupled lines, respectively, and Z_{t2} is the characteristic impedance of the open-circuit stub. For simplicity, the isolation structures are replaced by the isolators Z_{iso1} and Z_{iso2}. Based on (1), the phase shift φ and the equivalent characteristic impedance Z_c of the CL structure with an open-circuit stub can be derived as follows [14]:

$$\begin{aligned}|\varphi| &= \left|Arc\cos\left(\frac{Z_{ine}+Z_{ino}}{Z_{ine}-Z_{ino}}\right)\right| \\ &= \left|Arc\cos\left(\frac{(Z_{e2}^2+Z_{e2}Z_{o2}+2Z_{o2}Z_{t2})\tan^2\theta - 2Z_{e2}Z_{t2}}{(Z_{e2}^2-Z_{e2}Z_{o2}-2Z_{o2}Z_{t2})\tan^2\theta - 2Z_{e2}Z_{t2}}\right)\right|,\end{aligned} \tag{2a}$$

$$Z_c = \sqrt{Z_{ine}Z_{ino}} = \sqrt{\frac{Z_{e2}Z_{o2}(2Z_{t2} - Z_{e2}\tan^2\theta)}{Z_{e2} + 2Z_{t2}}}. \tag{2b}$$

As shown in Fig. 2(a), the odd-mode input impedances of the WFPD with the right-hand side excitation can be obtained as:

$$\begin{cases} Z_{ORin5} = jZ_{o1}\tan\theta \\ Z_{ORin4} = \dfrac{Z_{ORin5}Z_{iso1}}{2Z_{ORin5} + Z_{iso1}} \\ Z_{ORin3} = Z_c\dfrac{Z_{ORin4} + jZ_c\tan\varphi}{Z_c + jZ_{ORin4}\tan\varphi} \\ Z_{ORin2} = Z_{o3}\dfrac{Z_{ORin3} + jZ_{o3}\tan\theta}{Z_{o3} + jZ_{ORin3}\tan\theta} \\ Z_{ORin1} = jZ_{t1}\tan\theta_{t1} \\ Z_{ORin} = \dfrac{Z_{iso2}Z_{ORin1}Z_{ORin2}}{2Z_{ORin1}Z_{ORin2} + Z_{iso2}(Z_{ORin1} + Z_{ORin2})}. \end{cases} \tag{3}$$

Therefore, the reflection coefficient Γ^o_{out} at the output port 2 (or port 3) in the odd-mode equivalent circuit can be deduced as [8]:

$$\Gamma^o_{out} = \frac{Z_{ORin} - Z_0}{Z_{ORin} + Z_0}. \tag{4}$$

Similarly, the even-mode input impedances of the WFPD with the left-/right-hand side excitation in Figs. 2(b) and 2(c) can be obtained as:

$$\begin{cases} Z_{ELin4} = jZ_{t1}\tan\theta_{t1} \\ Z_{ELin3} = \dfrac{Z_{ELin4}Z_0}{Z_{ELin4} + Z_0} \\ Z_{ELin2} = Z_{e3}\dfrac{Z_{ELin3} + jZ_{e3}\tan\theta}{Z_{e3} + jZ_{ELin3}\tan\theta} \\ Z_{ELin1} = Z_c\dfrac{Z_{ELin2} + jZ_c\tan\varphi}{Z_c + jZ_{ELin2}\tan\varphi} \\ Z_{ELin} = Z_{e1}\dfrac{Z_{ELin1} + jZ_{e1}\tan\theta}{Z_{e1} + jZ_{ELin1}\tan\theta}, \end{cases} \tag{5}$$

and

$$\begin{cases} Z_{ERin4} = Z_{e1}\dfrac{2Z_0 + jZ_{e1}\tan\theta}{Z_{e1} + j2Z_0\tan\theta} \\ Z_{ERin3} = Z_c\dfrac{Z_{ERin4} + jZ_c\tan\varphi}{Z_c + jZ_{ERin4}\tan\varphi} \\ Z_{ERin2} = Z_{e3}\dfrac{Z_{ERin3} + jZ_{e3}\tan\theta}{Z_{e3} + jZ_{ERin3}\tan\theta} \\ Z_{ERin1} = jZ_{t1}\tan\theta_{t1} \\ Z_{ERin} = \dfrac{Z_{ERin1}Z_{ERin2}}{Z_{ERin1} + Z_{ERin2}}. \end{cases} \tag{6}$$

Hence, the reflection coefficient Γ^e_{in} at the input port 1 and Γ^e_{out} at the output port 2 (or port 3) for the even-mode equivalent circuit can be deduced as:

$$\Gamma^e_{in} = \frac{Z_{ELin} - 2Z_0}{Z_{ELin} + 2Z_0}, \tag{7a}$$

$$\Gamma^e_{out} = \frac{Z_{ERin} - Z_0}{Z_{ERin} + Z_0}. \tag{7b}$$

In order to achieve an excellent in-band return loss, the ultra-wide stopband, and isolation frequency band, the S-parameters of the proposed WFPD can be calculated as:

$$S_{11} = \Gamma^e_{in}, \tag{8a}$$

$$S_{23} = \frac{\Gamma^e_{out} - \Gamma^o_{out}}{2}. \tag{8b}$$

Therefore, by defining the S_{11}, the input return loss and the passband bandwidth can be determined based on the two CL sections. With $\theta_1 = \theta_2 = \theta_3 = \theta_{t2} = \theta_{t1}/4 = \theta$, an ultra-wide stopband with several transmission zeros can be obtained. Hereinto, the locations of three fixed transmission zeros generated from short-circuit stubs can be found by solving:

$$f_{zn} = \left(\frac{n\cdot 45^\circ}{\theta}\right)\cdot f_0, \quad n = 1, 2, 3 \tag{9}$$

where θ is now considered in degrees and not in radians anymore. Additionally, the other two transmission zeros are created by the CLs with an open-circuit stub. Moreover, the locations of the other two transmission zeros can be tuned by the characteristic impedances of the CLs with the open-circuit stubs (Z_{e2} and Z_{o2}). The design equations can be derived by using $S_{21} = 0$, whereas the complex and tedious equations are difficult to be solved. For depicting the presence and the control of the transmission zeros clearly, four ideal simulated cases operating at 1 GHz for different transmission zeros in the stop band are implemented with different design parameters in Fig. 3. Fig. 3(a) illustrates the input return loss and the insertion loss of the four ideal simulated cases. Furthermore, in order to maintain the same bandwidth of the 20-dB in-band return loss, the characteristic impedances of CLs and short-circuit stubs are adjusted. For Cases 1, 2, 3, and 4, the transmission zeros are at (i) 2 GHz, 4 GHz, and 6 GHz; (ii) 2 GHz, 3.5 GHz, 4 GHz, 4.5 GHz, and 6 GHz; (iii) 2GHz, 3 GHz, 4 GHz, 5 GHz, and 6 GHz, and (iv) 2GHz,

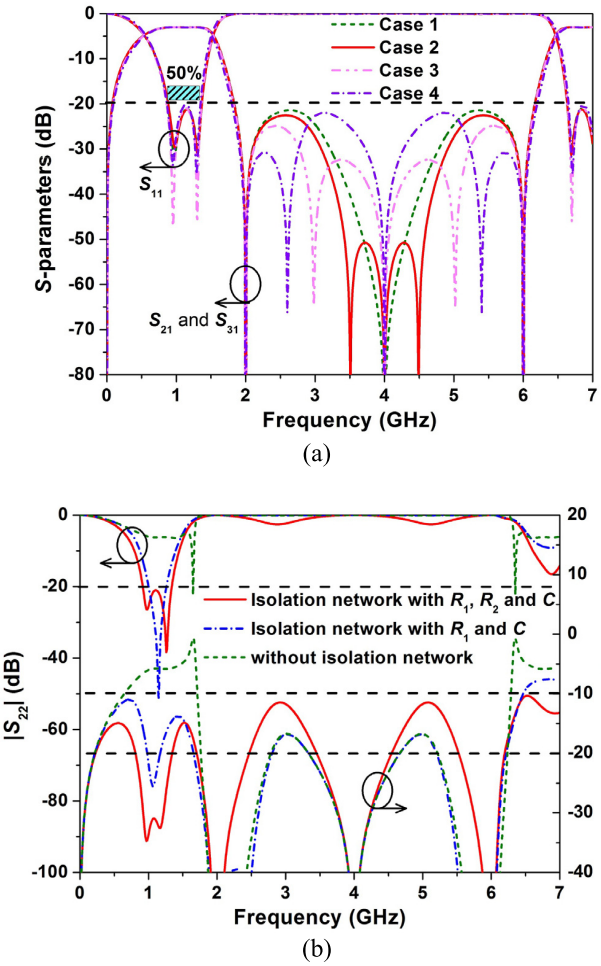

FIGURE 3. The *S*-parameters of the ideal simulated cases operating at 1 GHz with different transmission zeros in the stop band. (a) The magnitude of S_{11} and S_{21}. (b) The magnitude of S_{22} and S_{23} with different isolation networks for Case 2.

TABLE 1. The corresponding characteristic impedances of the simulated cases with different transmission zeros in Fig. 3(a).

	Z_{e1} (Ω)	Z_{o1} (Ω)	Z_{e2} (Ω)	Z_{o2} (Ω)	Z_{e3} (Ω)	Z_{o3} (Ω)	Z_{t1} (Ω)	Z_{t2} (Ω)
Case 1	130	80	123	55	110	85	40	78
Case 2	130	80	128	55	110	85	40	78
Case 3	110	91	139	54	100	78	37	75
Case 4	108	88	148	45	106	91	34	76

2.6 GHz, 4 GHz, 5.4 GHz, and 6 GHz, respectively. Moreover, the bandwidth of the 20-dB in-band return loss is about 50% from 0.86 to 1.36 GHz for all cases. In other words, maintaining the in-band return loss (S_{11}) better than 20 dB and a wide passband of 50%, the ultra-wide stopband with the 6th harmonic suppression is below −20 dB within the range of 2 GHz to 6 GHz. The corresponding design parameters of these cases are summarized in Table I.

As shown in Fig. 3(b), in the case of no isolation network, the proposed circuit configuration can provide a broad out-of-band isolation. Therefore, in order to improve the in-band isolation between the output ports, based on (3), (4), and (6)-(8), the general isolation network can be calculated as:

$$\begin{aligned} Z_{iso1} &= \frac{2jZ_cZ_{ORin5}[\tan\theta(jaZ_{o3}^2 - jZ_{ORin1}(bZ_{o3}^2 - jac)) + jZ_{o3}g]}{Z_cZ_{o3}g + \tan\theta[jdZ_{ORin5} + Z_cae + jZ_{ORin1}(jZ_cbe + ah)]} \\ &= R_1 + 1/(j\omega C) \end{aligned} \tag{10}$$

where

$$a = Z_{ERin}Z_{iso2}, \tag{11a}$$
$$b = -2Z_{ERin} + Z_{iso2}, \tag{11b}$$
$$c = Z_c\tan\varphi, \tag{11c}$$
$$d = (aZ_{o3}^2\tan\varphi - jZ_{ORin1}(Z_ca - jbZ_{o3}^2\tan\varphi)), \tag{11d}$$
$$e = Z_{o3}(Z_{o1} + Z_{o3}), \tag{11e}$$
$$g = ac - Z_{ORin1}(ja + bc), \tag{11f}$$
$$h = (Z_c^2 + Z_{o1}Z_{o3})\tan\varphi. \tag{11g}$$

From (10) and (11), the series connected *RC* network should be utilized to achieve high in-band isolation. As shown in Fig. 3(b), when the isolation network only adopts the series *RC*, the in-band isolation can be improved without affecting the out-of-band isolation. For further extending the bandwidth of in-band isolation, a single resistor located between the two output ports is utilized, while the out-of-band isolation is attenuated to 10 dB. Finally, the in-band isolation of Case 2 is better than 20 dB from 0.81 GHz to 1.34 GHz for the isolation network with R_1, R_2 and C, and the 10 dB absolute bandwidth of isolation is 7 GHz. Moreover, the output matching is better than 20 dB from 0.92 GHz to 1.34 GHz. Therefore, we have achieved the good output matching performance ($|S_{22}| < -20$ dB), the perfect in-band isolation ($|S_{23}| < -20$ dB) and the ultra-wide isolation frequency band (0-7 GHz) for R_1, R_2, and C values of 30 Ω, 300 Ω and 2.5 pF, respectively.

B. DESIGN PROCEDURE

The design procedure of the proposed WFPD can be summarized as follows:

1) Determine the operating frequency f_0 and the locations of transmission zeros according to (9).
2) Based on (4), (7), and (8), the even-/odd-mode impedances of CLs with open-circuit stubs and the characteristic impedances of short-circuit stubs can be determined.
3) Select the proper resistors (R_1, R_2) and capacitor C, improved output matching, high in-band isolation, and ultra-wide isolation frequency band can be achieved by (10) and (11).

III. IMPLEMENTATION AND MEASURED RESULTS

In this section, the simulated results are obtained by using the Advanced Design System (ADS) tool based on the method of moments (MOM). Furthermore, the required circuit layout is fabricated on the top layer of a RO4350B substrate, whereas the ground is placed on the bottom layer of the substrate.

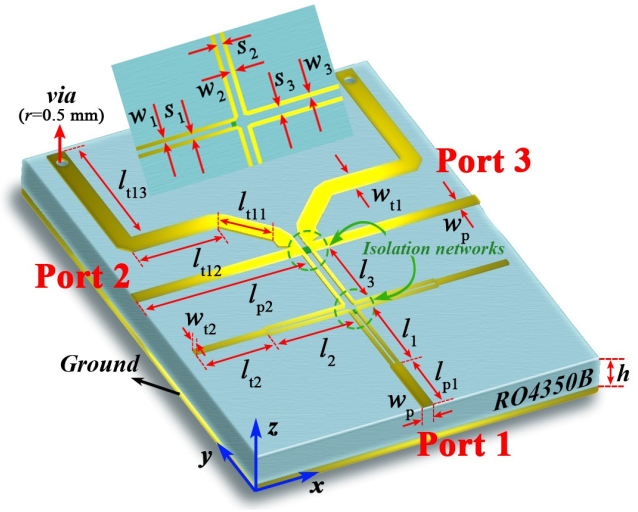

FIGURE 4. The corresponding circuit layout of the proposed filtering power divider on the substrate of RO4350B.

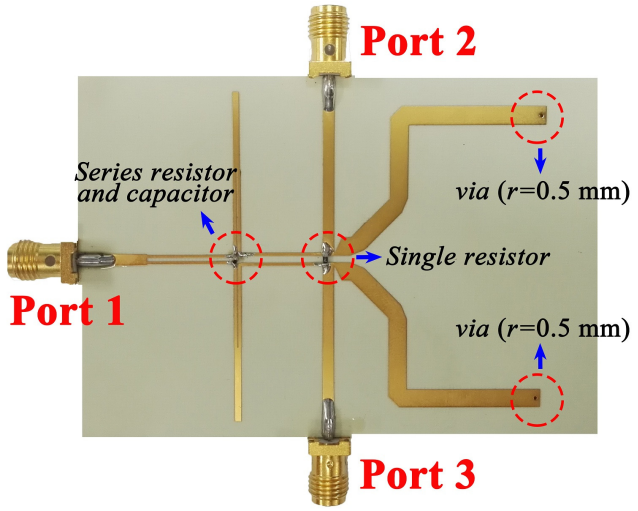

FIGURE 5. The photograph of the fabricated WFPD. The input and output ports are terminated with 50-Ω SMA connectors and the two via holes are used for the ground connection.

Moreover, the metal thickness of each layer is about 35 μm. Finally, with the help of a vector network analyzer, we have measured the circuit model of the designed WFPD.

For further theoretical verification, the Case 2 in Fig. 3 is fabricated and measured based on a substrate of the relative permittivity ε_r, the thickness h and the loss tangent of 3.48, 0.762 mm, and 0.0037, respectively. The corresponding circuit layout and photograph of the fabricated WFPD are depicted in Fig. 4 and Fig. 5, respectively. As shown in Fig. 4, the circuital dimensions of the proposed WFPD at the operating frequency of 1 GHz are optimized and are (all in millimeters): $w_p = 1.72$, $w_1 = 0.44$, $w_2 = 0.48$, $w_3 = 0.49$, $w_{t1} = 2.8$, $w_{t2} = 0.96$, $l_{p1} = 10$, $l_1 = 13$, $l_2 = 12.91$, $l_3 = 12.47$, $l_{t11} = 8.3$, $l_{t12} = 12.2$, $l_{t13} = 21.9$, $l_{t2} = 11.5$, $l_{p2} = 27$, $s_1 = 0.53$, $s_2 = 0.18$, $s_3 = 1.04$, $h = 0.762$, and $r = 0.5$. Herein, the two via holes with the radius of 0.5 mm

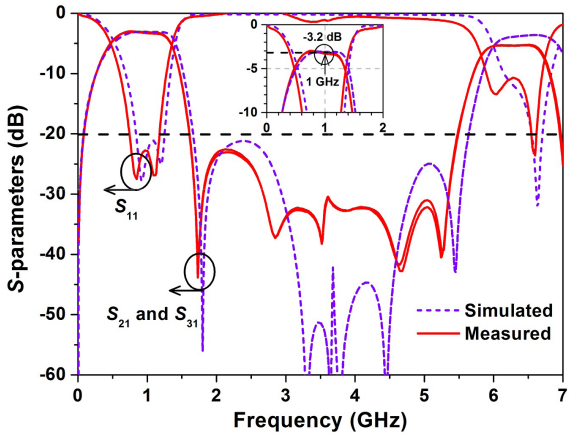

(a)

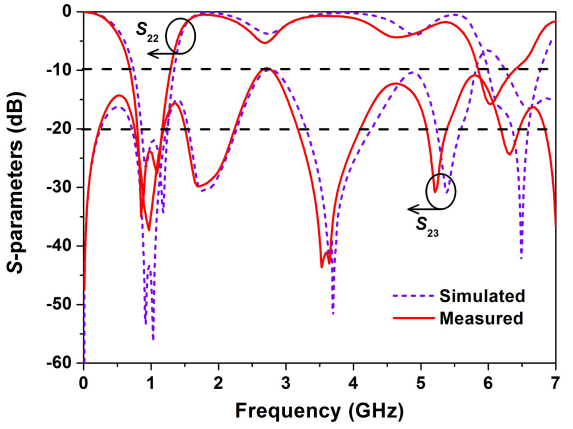

(b)

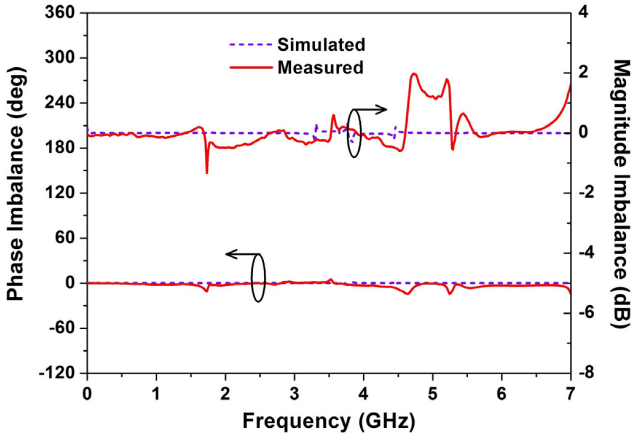

(c)

FIGURE 6. The EM simulated and measured results of the proposed WFPD: (a) the magnitude of S_{11}, S_{21} and S_{31}, (b) the magnitude of S_{22} and S_{23}, and (c) phase imbalance and magnitude imbalance.

are used for the ground connection to achieve the equivalent short-circuited function. Additionally, the values of R_1, R_2 and$C$ are selected as 30 Ω, 240 Ω, and 3 pF, respectively in the practical measurements.

Fig. 6 displays the EM simulated and measured results. As shown in Fig. 6(a), the measured bandwidth

TABLE 2. Performance comparison of filtering power dividers.

Refs.	The center frequency f_0 (GHz)	FBW/RL[1] (Inband)	BW/IL[2] (Stopband)	In-band IL[2] (dB)	Isolation (Inband)	Isolation (Out of band)	TZs[3] (Out of band)	Size ($\lambda_g \times \lambda_g$)	Years
[1]	1.8	9.4% 10 dB	-	3.9	10 dB	Wide	1	0.45×0.54	2013
[2]	1	6.7% 10 dB	-	3.8	20 dB	Wide	2	0.17×0.25	2014
[3]	1.2	3.5% 16 dB	-	4.4	30 dB	Wide	1	0.19×0.19	2014
[4]	2.4	4.1% 10 dB	1.8 f_0 15 dB	4.2	10 dB	Narrow	1	0.45×0.45	2015
[5]	1.4	9.5% 10 dB	6 f_0 30 dB	4.3	16 dB	Ultra-wide	3	0.13×0.19	2016
[6]	0.9	22.2% 10 dB	22.2 f_0 10 dB	3.7	20 dB	-	-	0.1×0.2	2014
[7]	2.5	6% 10 dB	0.9 f_0 20 dB	4.3	-	-	2	0.15×0.3	2014
[8]	3	104.5% 15 dB	3.4 f_0 15 dB	3.7	15 dB	Ultra-wide	3	0.2×0.15	2016
This work	**1**	**43% 20 dB**	**3.9 f_0 20 dB**	**3.2**	**20 dB**	**Ultra-wide**	**5**	**0.43×0.34**	**2016**

[1]RL: Return loss; [2]IL: Insertion loss; [3]TZs: Transmission zeros

of 20-dB in-band return loss is about 43% across the band of 0.75–1.18 GHz. The measured magnitude of S_{21} and S_{31} at 1 GHz are about −3.173 dB and −3.306 dB, respectively, whereas the in-band amplitude imbalance illustrated in Fig. 6(c) between the two output ports is about 0.1 dB. Moreover, in Fig. 6(a) the measured stopband is below −20 dB from 1.6–5.5 GHz with harmonic suppression located at 1.73 GHz, 2.85 GHz, 3.52 GHz, 4.64 GHz, and 5.28 GHz. Additionally, from Fig. 6(b) the measured in-band isolation is better than 20 dB ranged from 0.76-1.18 GHz while out-of-band isolation is greater than 10 dB. The phase difference at 1 GHz is about 1.823° from Fig. 6(c). From the aforementioned results, we can see that the excellent 20-dB return loss with a bandwidth of 43% is obtained under the conditions of maintaining the in-band isolation (S_{23}) and output matching (S_{22}) better than 20 dB. Moreover, the ultra-wide stopband with high harmonic suppression and ultra-wideband isolation are also achieved. Therefore, judging from the preceding results, good agreement between the simulated and measured results has been shown. In the end, the comparison of the presented WFPD with other designs is listed in Table II.

IV. CONCLUSION

In this paper, a wideband filtering power divider based on the CL sections and the short-/open-circuit stubs is proposed and discussed. Apart from major advantages of an excellent input return loss and a broad operating band with filtering response, the proposed filtering power divider displays an ultra-wide stopband with five transmission zeros and an ultra-wideband isolation. Therefore, it can be expected that this power divider will be widely applied in the modern wireless communication systems.

ACKNOWLEDGMENT

In addition, the corresponding Chinese patent (No. 201610308677.0) of the part of odd-/even-mode circuit has been pending.

REFERENCES

[1] Y. C. Li, Q. Xue, and X. Y. Zhang, "Single- and dual-band power dividers integrated with bandpass filters," *IEEE Trans. Microw. Theory Techn.*, vol. 61, no. 1, pp. 69–76, Jan. 2013.

[2] S.-F. Chao and Y.-R. Li, "Miniature filtering power divider with increased isolation bandwidth," *Electron. Lett.*, vol. 50, no. 8, pp. 608–610, Apr. 2014.

[3] C.-F. Chen and C.-Y. Lin, "Compact microstrip filtering power dividers with good in-band isolation performance," *IEEE Microw. Wireless Compon. Lett.*, vol. 24, no. 1, pp. 17–19, Jan. 2014.

[4] K. Song, "Compact filtering power divider with high frequency selectivity and wide stopband using embedded dual-mode resonator," *Electron. Lett.*, vol. 51, no. 6, pp. 495–497, Mar. 2015.

[5] X.-L. Zhao, L. Gao, X. Y. Zhang, and J.-X. Xu, "Novel filtering power divider with wide stopband using discriminating coupling," *IEEE Microw. Wireless Compon. Lett.*, vol. 26, no. 8, pp. 580–582, Aug. 2016.

[6] W.-M. Chau, K.-W. Hsu, and W.-H. Tu, "Wide-stopband Wilkinson power divider with bandpass response," *Electron. Lett.*, vol. 50, no. 1, pp. 39–40, Jan. 2014.

[7] K. Song, X. Ren, F. Chen, and Y. Fan, "Compact in-phase power divider integrated filtering response using spiral resonator," *IET Antennas Propag. Microwaves*, vol. 8, no. 4, pp. 228–234, Mar. 2014.

[8] C.-W. Tang and J.-T. Chen, "A design of 3-dB wideband microstrip power divider with an ultra-wide isolated frequency band," *IEEE Trans. Microw. Theory Techn.*, vol. 64, no. 6, pp. 1806–1811, Jun. 2016.

[9] K.-X. Wang, X. Y. Zhang, and B.-J. Hu, "Gysel power divider with arbitrary power ratios and filtering responses using coupling structure," *IEEE Trans. Microw. Theory Techn.*, vol. 62, no. 3, pp. 431–440, Mar. 2014.

[10] C. Cai, J. Wang, Y. Deng, and J.-L. Li, "Design of compact dual-mode dual-band filtering power divider with high selectivity," *Electron. Lett.*, vol. 51, no. 22, pp. 1795–1796, Oct. 2015.
[11] L. Gao, X. Y. Zhang, and Q. Xue, "Compact tunable filtering power divider with constant absolute bandwidth," *IEEE Trans. Microw. Theory Tech.*, vol. 63, no. 10, pp. 3505–3513, Oct. 2015.
[12] F.-J. Chen, L.-S. Wu, L.-F. Qiu, and J.-F. Mao, "A four-way microstrip filtering power divider with frequency-dependent couplings," *IEEE Trans. Microw. Theory Techn.*, vol. 63, no. 10, pp. 3494–3504, Oct. 2015.
[13] K. Song, Y. Mo, and Y. Fan, "Wideband four-way filtering-response power divider with improved output isolation based on coupled lines," *IEEE Microw. Wireless Compon. Lett.*, vol. 24, no. 10, pp. 674–676, Oct. 2014.
[14] B. Li, X. Wu, N. Yang, and W. Wu, "Dual-band equal/unequal Wilkinson power dividers based on coupled-line section with short-circuited stub," *Prog. Electromag. Res.*, vol. 111, pp. 163–178, 2011.

YONGLE WU (M'12–SM'15) received the B.Eng. degree in communication engineering and the Ph.D. degree in electronic engineering from the Beijing University of Posts and Telecommunications (BUPT), Beijing, China, in 2006 and 2011, respectively.

In 2010, he was a Research Assistant with the City University of Hong Kong, Kowloon, Hong Kong. In 2011, he joined BUPT and is currently an Associate Professor with the School of Electronic Engineering. His research interests include microwave components and wireless systems design.

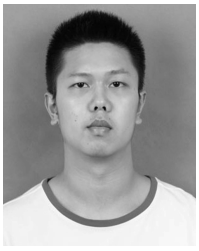

ZHENG ZHUANG received the B.S. degree in electronic science and technology from the Beijing University of Chemical Technology, Beijing, China, in 2015. He is currently pursuing the M.S. degree with the Beijing University of Posts and Telecommunications (BUPT). In 2015, he started his research as a Graduate with BUPT.

His research interests include microwave passive components and power amplifiers.

YUANAN LIU received the B.E., M.Eng., and Ph.D. degrees in electrical engineering from the University of Electronic Science and Technology of China, Chengdu, China, in 1984, 1989, and 1992, respectively.

In 1984, he joined the 26th Institute of Electronic Ministry of China to develop the inertia navigating system. In 1992, he started his first post-doctor position with the EMC Laboratory, Beijing University of Posts and Telecommunications (BUPT), Beijing, China. In 1995, he started his second post-doctor position with the Broadband Mobile Laboratory, Department of System and Computer Engineering, Carleton University, Ottawa, Canada. Since 1997, he has been a Professor with the Wireless Communication Center, College of Telecommunication Engineering, BUPT, where he is involved in the development of the next-generation cellular system, wireless LAN, Bluetooth application for data transmission, EMC design strategies for high-speed digital system, and electromagnetic interference and electromagnetic susceptibility measuring sites with low cost and high performance. He is interested in smart antennas for high-capacity mobile signal processing techniques in fading environments, EMC for high-speed digital system, ISI suppression, orthogonal frequency division multiplexing, and multicarrier system design. He is a Senior Member of the Electronic Institute of China.

LI DENG was born in Sichuan, China, in 1982. He received the B.Eng. and M.Eng. degrees in communication engineering from Beijing Jiaotong Universtiy in 2004 and 2007, respectively, and the Ph.D. degree in communication engineering from the Beijing University of Posts and Telecommunications (BUPT), Beijing, China, in 2010.

In 2012, he joined BUPT, where he is currently an Associate Professor with the School of Information and Communication Engineering. His research interests include electromagnetic theory, metamaterial, and transformation optics.

ZABIH GHASSEMLOOY (SM'02) received the B.Sc. degree (Hons.) in electrical and electronics engineering from Manchester Metropolitan University in 1981 and the M.Sc. and Ph.D. degrees in optical communications from the University of Manchester, U.K., in 1984 and 1987, respectively. From 1987 to 1988, he was a Post-Doctoral Research Fellow with City University, London, U.K. In 1988, he joined Sheffield Hallam University as a Lecturer, and became a Professor of optical communications in 1997. He is currently with Northumbria University, Newcastle, heading the Northumbria Communications Research Laboratory. His research interests are in optical wireless communications, free space optics, and visible light communications.